

RSC Advances

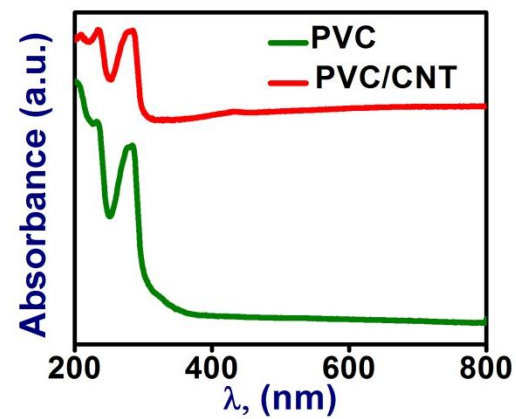
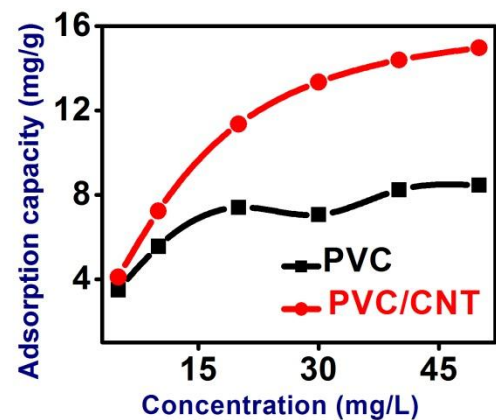
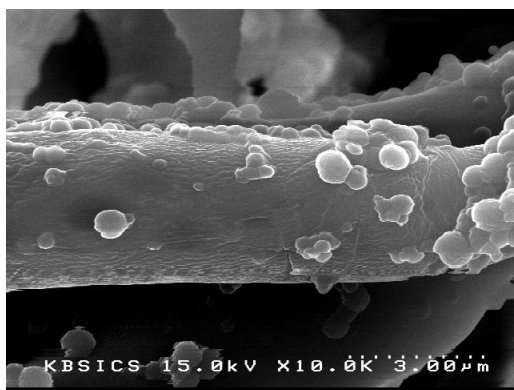


This is an *Accepted Manuscript*, which has been through the Royal Society of Chemistry peer review process and has been accepted for publication.

Accepted Manuscripts are published online shortly after acceptance, before technical editing, formatting and proof reading. Using this free service, authors can make their results available to the community, in citable form, before we publish the edited article. This *Accepted Manuscript* will be replaced by the edited, formatted and paginated article as soon as this is available.

You can find more information about *Accepted Manuscripts* in the [Information for Authors](#).

Please note that technical editing may introduce minor changes to the text and/or graphics, which may alter content. The journal's standard [Terms & Conditions](#) and the [Ethical guidelines](#) still apply. In no event shall the Royal Society of Chemistry be held responsible for any errors or omissions in this *Accepted Manuscript* or any consequences arising from the use of any information it contains.



A novel deposition route for PVC/CNT nanocomposite fibers synthesis and its application towards ARS removal

ARTICLE

Synthesis of PVC/CNT nanocomposite Fibers using simple deposition technique for the application of Alizarin Red S (ARS) removal[†]

Cite this: DOI: 10.1039/x0xx00000x

Mudassir Hasan^a, Rajeev Kumar^{b*}, M.A. Barakat^{bc}, Moonyong Lee^{a*}

Received 00th January 2012,
Accepted 00th January 2012

DOI: 10.1039/x0xx00000x

www.rsc.org/

This paper reports the synthesis of PVC/CNT nanocomposite fibers using a simple deposition technique as well as its application towards removal of Alizarin Red S (ARS). The as-prepared PVC/CNT nanocomposite fibers were characterized by Brunauer, Emmett and Teller surface area measurements, Raman spectroscopy, X-ray photoelectron spectroscopy, X-ray diffraction, transmission electron microscopy, scanning electron microscopy, thermogravimetric analysis, differential scanning calorimetry and diffused reflectance spectroscopy. PVC/CNT nanocomposite fibers showed a remarkable 81% increase in surface area compared to the PVC fibers. PVC/CNT nanocomposite fibers showed a lower band gap and higher glass transition temperature than the PVC fibers. Both PVC and PVC/CNT nanocomposite fibers were applied to adsorb ARS and the nanocomposite fibers showed almost double the adsorption capacity than PVC fibers. The thermodynamic study revealed that adsorption of ARS was endothermic in nature and physical forces were involved in adsorption of dye onto PVC and PVC/CNT nanocomposite fibers.

Introduction

Recently, polymer/carbon nanotube (CNT) nanocomposites have become an important and interesting area of research worldwide. The obvious reason is because CNT have unique properties, such as low-weight, high aspect ratio¹, high mechanical properties² and high electrical³ and thermal conductivity.⁴ CNT have been used successfully to enhance the mechanical, thermal, optical and barrier properties of several polymer/ CNT nanocomposite structures.⁵⁻⁷ On the other hand, further systematic and optimized study of the physico-chemical properties of these polymer/CNT nanocomposites is necessary to find future applications for practical use.

Polyvinyl chloride (PVC) is one of the most versatile and widely used polymers after polyethylene. Moreover, it is chemically stable, biocompatible and relatively inexpensive polymer.⁸ One of the main problem that limits the practical use of the polymer is its lower thermal stability.⁹ Considerable work has been carried out over the past decade to enhance the thermal stability, mechanical strength and electrical conductivity of PVC using a range of nanofillers.¹⁰⁻¹⁴

Little information is available on the production of nanocomposite fibers of PVC with CNT.¹⁵ In industry, PVC fibers are produced using a range of techniques, such as wet-spinning, dry-spinning and melt-spinning. On the otherhand, these techniques have a range of limitations such as requirement of chemicals, need for high

temperature and higher cost. Therefore, before PVC/CNTs nanocomposite fibers can be used to replace the existing conventional method for the production of PVC fibers, more work will be needed to simplify the production technique and explore various characteristic properties of the PVC/CNTs nanocomposite fibers. Therefore, the aim of the present study was to prepare nanocomposite fibers of PVC with CNTs, and compare the physico-chemical properties with those of PVC/GN nanocomposite fibers. This research may be fruitful to people working in the area of polymer nanocomposites for practical use. In this study, PVC/CNTs nanocomposite fibers were prepared using a simple and facile deposition route. The structure, morphology, thermal stability, optical, and adsorption properties were also examined.

Experimental

Materials

PVC (average molecular weight ~1020) was purchased from Yakuri pure chemicals, Japan and MWCNT (diameter ~10-20 nm and average length ~20 μm with 95% purity) was purchased from Hanwha Nanotech, Korea. Tetrahydrofuran (THF) was supplied by Duksan pure chemicals, Korea, and used as received. Alizarin Red S (ARS) [C.I., 58005, M.F.: $\text{C}_{14}\text{H}_7\text{NaO}_7\text{S}$] was purchased from BDH chemicals LTD, England.

Preparation and characterization of PVC, PVC/CNT nanocomposite fibers

Structural analyses of the samples were carried out by X-ray diffraction (XRD, PAN analytical, X'pert PRO-MPD) in the range, $10\text{-}90^\circ 2\theta$, using Cu $K\alpha$ radiation ($\lambda = 0.15405$ nm). Raman spectroscopy (InVia Reflex UV Raman microscope, Renishaw, UK) was employed to examine the defects created on the lattice of CNTs in the PVC/CNT nanocomposite fibers. X-ray photoelectron spectroscopy (XPS, ESCALAB 250) was performed using a monochromatized Al $K\alpha$ X-ray source ($h\nu = 1486.6$ eV) with a 500 μm spot size. Scanning electron microscopy (SEM, Hitachi-4200) was employed to examine surface morphology. The optical properties were obtained by ultraviolet-visible-near infrared (UV-VIS-NIR, VARIAN, Cary 5000, USA) spectrophotometry. The microstructure was analyzed by field emission transmission electron microscopy (FE-TEM, TecnaiG2 F20, FEI, USA) operating at an accelerating voltage of 200 KV. Thermogravimetric analysis (TGA, SDT Q600, USA) was performed by heating the samples from 25°C to 800°C at a rate of $10^\circ\text{C min}^{-1}$ in a nitrogen atmosphere. Differential scanning calorimetry (DSC, Q 200, USA) was performed by heating the samples from 20°C to 200°C . Quantachrome, Asic-7 physisorption analyzer was used to estimate the surface area of fibers while the pore size and pore volume were obtained using the Barrett Joyner Halenda (BJH) theory.

The adsorption experiments were conducted by taking 20 mL of the dye solution in a series of flasks containing 0.02 g adsorbent fibers at 30°C and the dye concentration was varied from 5 to 50 mg/L. For the thermodynamic studies, 0.02 g fibers were added to the flask containing 20 mL of an 20 mg/L ARS solution with shaking at 200 rpm at varying temperatures ($30, 40$ and 50°C). The amount of ARS remaining in the supernatant solution was determined using HACH LANGE DR 6000 UV-visible spectrophotometer at 423 nm. The adsorption capacity of polymeric fibers for ARS was calculated using following equation:

$$q_e = (C_0 - C_e)V/m \quad (1)$$

where q_e is the amount of ARS adsorbed per unit mass of fiber (mg g^{-1}), C_0 and C_e is the initial and equilibrium ARS concentration (mg L^{-1}), respectively. V is the volume of ARS solution (L) and m is the mass of the fiber (g).

Preparation of the PVC/CNT nanocomposite fibers

The PVC/CNT nanocomposite fibers were prepared in two steps: the synthesis of PVC/CNT nanocomposites by mixing CNT in a THF solution of PVC followed by a deposition technique to prepare the PVC/CNT nanocomposite fibers. In a typical process, PVC was first dissolved in 50 mL of THF with continuous stirring for 24 hours for complete dissolution. The CNTs were mixed with the above solution with continuous stirring and occasional shaking in bath ultrasonic system for 5 minutes to allow proper dispersion of CNTs inside the THF solution of PVC. Subsequently, the mixture was poured into distilled water with vigorous stirring to obtain the PVC/CNT nanocomposite fibers. The fibers were washed with

distilled water and an excess of methanol, and later dried at 60°C in an air oven for 24 hours. Pure PVC fibers were also prepared using a similar route in the absence of CNT. Table S1 lists the preparation conditions.

Results and discussion

Methods

A simple facile deposition technique was used to prepare PVC/CNT nanocomposite fibers using two immiscible solvent systems, i.e. THF and water. The PVC/CNT dispersed in THF solvents with vigorous stirring precipitated readily in water because of its insolubility in water. The surface area of the fibers was expected to increase after incorporating the CNTs into the PVC matrix due to the high surface area of nanomaterials, which is desirable for the surface-related properties, such as adsorption and catalysis.

X-ray diffraction

Fig. 1 shows XRD patterns of the PVC/CNT nanocomposite fibers. The XRD patterns of the PVC/CNT nanocomposite fibers (Fig. 1) showed no clear peak of PVC and CNT, which might be due to the encapsulation of CNT by the dense fibrous structure PVC. Hasan et al.¹⁶ reported a similar effect of encapsulation by PVC fibers on PVC/Graphene nanocomposite fibers. In this case, the XRD pattern clearly revealed the complete reduction and diffusion of the peak intensities because of the fibrous structure of PVC/CNT nanocomposites.

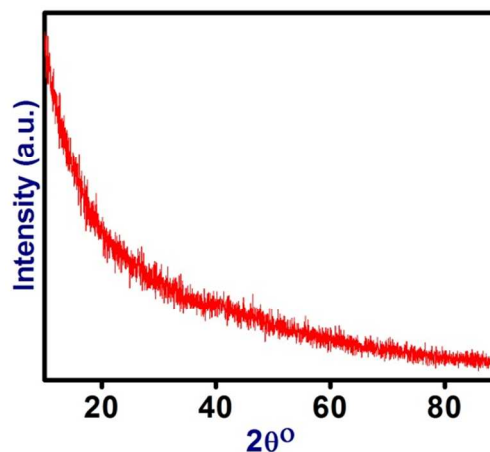


Fig. 1 XRD patterns of the PVC/CNT fibers

Raman analysis

Raman spectroscopy was used for qualitative investigation of the structural defects created on the lattices of CNTs present in the PVC/CNT nanocomposite system. The Raman spectra (Fig. 2) of the PVC/CNT nanocomposite fibers showed two characteristic bands, the D band that can be attributed to the vibration of sp^2 -bonded carbon atoms in a two-dimensional hexagonal lattice and G band, which can be attributed to scattering from the sp^3 -hybridized carbon

defects in the hexagonal framework of CNTs wall.¹⁷ The band intensity ratio (I_D/I_G) of the PVC/CNT nanocomposite, which is suggestive of the degree of covalent functionalization of the CNTs can be used for a qualitative estimation of the structural defects created on the lattice of CNTs. The intensity ratio between the D- and G-bands (I_D/I_G) was calculated to be 0.93 and 0.84 for PVC/CNT nanocomposite fibers and pristine CNTs, respectively. The band intensity ratio ($I_D/I_G \approx 1$) indicates considerable lattice defects.¹³ The observed increase in the I_D/I_G ratio of the PVC/CNT nanocomposite fibers compared to the CNTs confirmed the enhancement in the structural defects in the lattice of CNTs. Owing to structural defects created in the lattice of CNTs, property of PVC/CNT nanocomposite fibers is expected to be different from the neat PVC fibers.

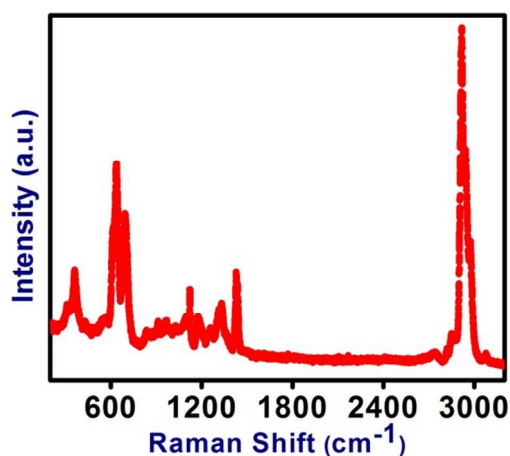


Fig. 2 Raman spectra of the PVC/CNT nanocomposite fibers

SEM and TEM analysis

Fig. 3a and 3b present SEM images of PVC and PVC/CNT nanocomposite fibers, respectively. Both PVC and PVC/CNT nanocomposite showed a clear image of the long stranded fibers with loose cotton like morphology. The average diameter of the fibers was measured to be $\sim 0.23 \mu\text{m}$. The loose cotton like morphology would increase the surface area of the PVC and PVC/CNT nanocomposite fibers, which was confirmed by BET surface area measurements, suggesting the suitability of the method for the preparation for the fibrous structures.

Fig. 3c presents TEM images of the PVC/CNT nanocomposite fibers. The low-magnification TEM images (Fig. 3c) clearly showed the PVC/CNT nanocomposite fibers attached to the wall of the CNTs. In addition, the mean thickness and length of the PVC/CNT nanocomposite fibers was measured to be 0.3 and $1 \mu\text{m}$, respectively (Fig. 3c). The TEM images of the nanocomposite fibers clearly revealed the successful incorporation of CNTs inside PVC, which may give rise to an enhanced glass transition temperature (Fig. 5) and increased surface area (Fig. 7).

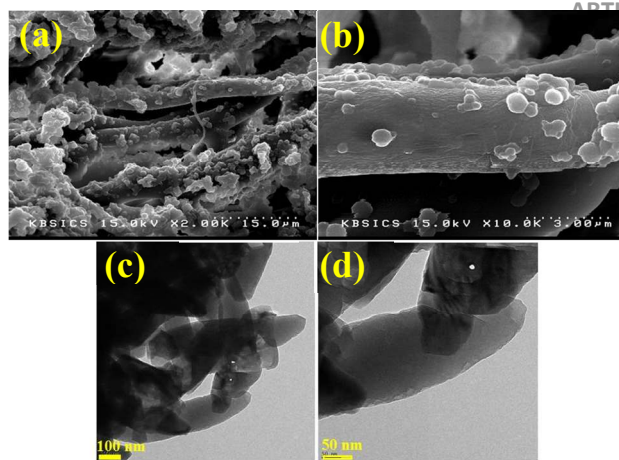


Fig. 3 SEM images of (a) PVC/CNT at $15 \mu\text{m}$ and (b) PVC/CNT at $3 \mu\text{m}$. (c) and (d) TEM images of PVC/CNT nanocomposite fibers at 100 and 50 nm.

Thermogravimetric analysis

Fig. 4 shows the TGA curves of the PVC and PVC/CNT nanocomposite fibers. The weight loss below $150 \text{ }^\circ\text{C}$ for both PVC and PVC/CNT nanocomposite fibers can be assigned to the evaporation of volatile components and trapped THF. Both PVC and PVC/CNT nanocomposite fibers degraded in two stages. In the first stage a weight loss of 65.85 and 58.03% was observed for the PVC and PVC/CNT nanocomposite fibers, respectively. The PVC and PVC/CNT nanocomposite fibers showed the first stage weight loss over the temperature range, $270\text{--}415$ and $260\text{--}418 \text{ }^\circ\text{C}$, respectively and can be attributed to the loss of HCl.¹⁵ In the second stage a weight loss of 16.63 and 17.87% was observed in the case of the PVC and PVC/CNT nanocomposite fibers, respectively, which took place over the temperature ranges, $425\text{--}550$ and $420\text{--}540 \text{ }^\circ\text{C}$, respectively. The second stage of weight loss was much shorter than the first stage and could be attributed to thermal degradation of the polyene backbone, resulting in the formation of volatile aromatic compounds and a stable carbonaceous residue.¹⁹ Finally a residual weight of 16.41 and 21.78% was observed in case of the PVC and PVC/CNT nanocomposite fibers, respectively, confirming the enhanced thermal stability of PVC/CNT nanocomposite fibers.

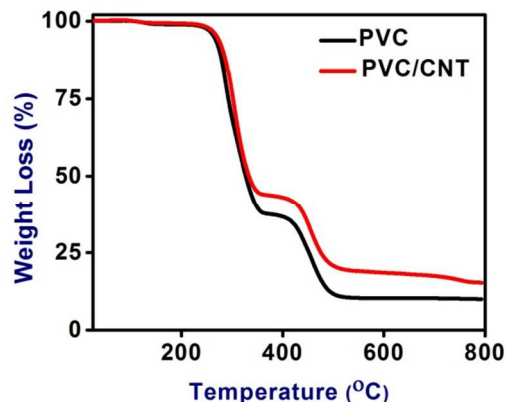


Fig. 4 TGA data of the PVC and PVC/CNT nanocomposite fibers

In addition, the CNTs are highly thermal stable might have imparted enhanced thermal stability to the PVC/CNT nanocomposite fibrous system, which might be due to the better thermal stabilization between the CNTs and PVC. Similar work was also reported by Hasan *et al.*²⁰

Differential scanning calorimetry

Fig. 5 shows the DSC thermograms of the PVC and PVC/CNT nanocomposite fibers. A hump relaxation, which is the characteristic for glass transition temperature (T_g), at around 79-84 °C for PVC and PVC/CNT nanocomposite fibers was shown by the plot between the heat flow rate versus temperature. T_g of the PVC and PVC/CNT nanocomposite fibers were found to be 81 and 82 °C respectively. Therefore, CNTs although very low in quantity, had some effect on the glass transition temperature of PVC/CNT nanocomposite fibers. The increase in T_g can be interpreted as the reinforcing effect of CNTs, which reduces the chain segmental mobility of PVC backbone.¹⁴ Table. 1 list the other thermal properties of interest, such as the onset (T_o), peak temperature (T_p) along with the glass transition temperature (T_g).

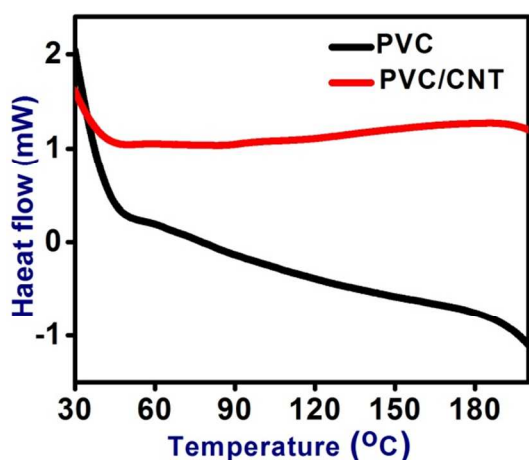


Fig. 5 DSC thermograms of PVC and PVC/CNT nanocomposite fibers

Table 1 Onset and peak temperatures as well as T_g of the PVC and PVC/CNT nanocomposite fibers

Sample name	$T_{o,m}$ (°C)	$T_{p,m}$ (°C)	T_g (°C)
PVC	234	294	81
PVC/CNT	268	302	82

Optical Properties

Both PVC and PVC/CNT nanocomposite fibers showed strong absorption in the UV region (Fig. 6). The PVC/CNT nanocomposite fiber showed considerably greater absorption compared to PVC fiber at wavelength $\lambda = 280$ nm. The absorbance of PVC/CNT nanocomposite fiber showed an enhancement of 56% with the CNT loading of 3 wt. % in PVC. Interestingly, with the same loading, 3

wt.% of CNT and GN in PVC the absorption of PVC/CNT nanocomposite fiber was approximately 70% higher compared to the PVC/GN nanocomposite fiber.¹⁶ The absorbance spectra showed absorbance peaks at $\lambda = 234$ and 280 nm, which can be assigned to the $n-\pi^*$ and $\pi-\pi^*$ transition, respectively.

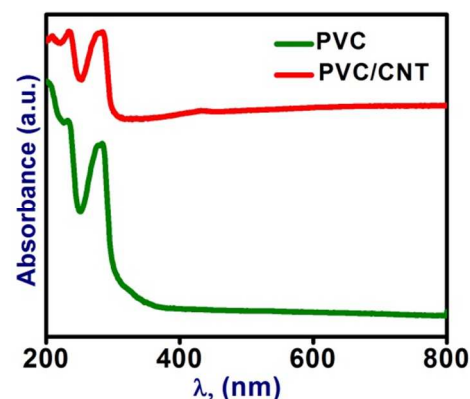


Fig. 6 UV-visible diffuse absorbance spectra of PVC and PVC/CNT nanocomposite fibers

The optical band gap of the PVC and PVC/CNT nanocomposite fibers was obtained using the approximate relationships among the reflectance (R), absorption coefficient (α), and scattering coefficient (s) based on Kubelka-Munk theory.²¹

$$\alpha = \frac{s}{2} \left(\frac{1-R}{R} \right)^2 \quad (2)$$

In above equation, α and s are functions of the energy of incident radiation ($h\nu$). The assumption was that s compared to α does not depend significantly on the wavelength at the absorption edge. Therefore, s was considered to be constant. The band gap of the PVC and PVC/CNT nanocomposite fibers was obtained from the absorption coefficient (α) using the following equation²²:

$$(\alpha h\nu)^{\frac{1}{x}} = A(h\nu - E_g) \quad (3)$$

This equation was formulated by the relationship for the parabolic bands at the onset of the absorption edge, where $h\nu$ is the incident photon energy, A is a material constant, and x is an exponent that depends on the type of transition. The value of x in the case of a direct allowed transition, indirect allowed transition and direct forbidden transition is 1/2, 2, 3/2, respectively. The band gap was determined by a plot of $(\alpha h\nu)^{\frac{1}{x}}$ and $h\nu$ at approximately the fundamental absorption region (Fig. S2 and S3)

Figs. S2 and S3 show the direct and indirect band gap calculation for the PVC and GN@PVC nanocomposite fibers. The direct and indirect allowed band gaps of all nanocomposite fibers were lower than those of PVC (Table S2). The estimated direct and indirect band gaps of PVC were 4.76 and 4.13 eV, respectively. Emad *et al.*²³ and Bushra *et al.*²⁴ reported similar direct and indirect band gaps for the PVC thin films. The decrease in the direct and indirect band gap in the present case for the PVC/CNT nanocomposite fibers were attributed to the formation of polarons in the fibers of the PVC loaded with CNTs. Some modifications in the size of the amorphous

domains in PVC due to the incorporation of CNTs can also explain the optical band gap reduction for the nanocomposite fibers.²⁵

Nitrogen Adsorption isotherms

The nitrogen adsorption isotherms of the PVC and PVC/CNT nanocomposite fibers were obtained (Fig. 7). Interestingly, both isotherms showed a hysteresis loop, confirming the characteristic feature of the type IV isotherms.²⁶ The isotherms of PVC fibers showed a very slow ascending section up to $p/p^0 = 0.61$. Afterwards it showed a slow descending section, which extended up to $p/p^0 = 0.91$. Finally, the isotherm showed an up-ward jump at saturation pressure $p/p^0 = 0.99$. On the other hand, the PVC/CNT nanocomposite fibers did not exhibit a descending section, showing a continuous slow ascending section up to $p/p^0 = 0.91$. A similar but an enhanced jump at a saturation pressure $p/p^0 = 0.99$ was observed. Nitrogen adsorption at high p/p^0 values was greater for the PVC/CNT nanocomposite fibers. The BET measurement clearly showed that the pores of the PVC/CNT nanocomposite fibers are micro porous. In addition, the BET surface area and pore volume of PVC/CNT nanocomposite fibers increased greatly (Table 2). Compared to PVC/GN nanocomposite fibers reported previously¹⁶, this materials showed an increase in the surface area and pore volume (Table 2).

Table 2 Physical properties deduced from N₂ adsorption at 77 K on PVC and PVC/CNT nanocomposite fibers.

Samples	Surface area (m ² /g)	Average pore volume (cm ³ /g)	Average pore diameter (nm)
PVC	2.018	5.467 x10 ⁻³	26.74
PVC/CNT	3.66	4.378 x10 ⁻²	16.40

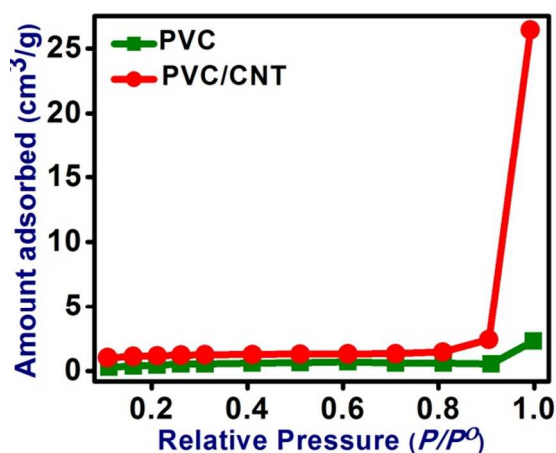


Fig. 7 N₂ adsorption isotherms of PVC and PVC/CNT nanocomposite fibers

Dye Adsorption studies

The efficiency of the PVC and PVC/CNT nanocomposite fibers for the removal of ARS was tested. The removal of ARS by using PVC and PVC-CNT fibers were increased from 3.5 to 9.5 mg/g and 4.1 to 14.9 mg/g, respectively, with increasing initial dye concentration from 5 to 50 mg/L as shown in Fig. 8. An increase in the initial ARS concentration may increase the driving force, which facilitates more ARS adsorption onto adsorbent fibers by minimization of the mass transfer resistance of the ARS molecules between the solid phase fibers and aqueous solution²⁷. The PVC/CNT nanocomposite fibers had almost double the adsorption capacity for ARS compared to PVC fibers. The higher adsorption capacity of PVC/CNT nanocomposite fibers than PVC was due mainly to the following two reasons: (i) the addition of CNTs to PVC may provide more open surface to the PVC matrix, which allows easy excess for ARS molecules to the adsorbent surface; (ii) the surface area of PVC/CNT was around 81% higher than PVC fibers which facilitated the higher adsorption; and (iii) the PVC/CNT nanocomposite fibers had more adsorption sites for ARS with an interaction through π - π interaction between CNTs and dye molecules.²⁸ For a better understating of surface property and interactions between ARS and fiber adsorbents, isotherm models, i.e., Langmuir, Freundlich and Temkin isotherm models were applied.

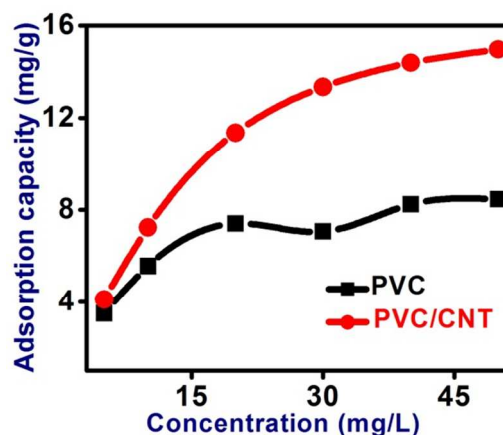


Fig. 8 Plot of adsorption capacity versus concentration for PVC and PVC/CNT nanocomposite fibers

The Langmuir isotherm model²⁹ is based on the assumption of monolayer adsorption onto an adsorbent surface that contains a finite number of identical active sites and no transmigration of the adsorbate in the plane of the surface. The linear equation for Langmuir isotherm is as follows:

$$\frac{1}{q_e} = \frac{1}{q_m b C_e} + \frac{1}{q_m} \quad (4)$$

where q_e (mg/g) is the amount of ARS adsorbed at equilibrium, C_e (mg/L) is the equilibrium concentration of ARS, q_m (mg/g) is the maximum monolayer adsorption capacity and b (L/mg) is the adsorption equilibrium constant. The Langmuir isotherm constants were calculated from a plot of $1/q_e$ versus $1/C_e$.

The Freundlich isotherm model³⁰ assumes that adsorption of adsorbate species occurs through a multilayer and heterogeneous system, characterized by the heterogeneity factor $1/n$. The linear equation for Freundlich isotherm is as follows:

$$\ln q_e = \ln K_F + \frac{1}{n} \ln C_e \quad (5)$$

where, K_F and n are the Freundlich constants, which indicate the adsorption capacity and adsorption intensity. The values of Freundlich isotherm parameters were calculated from a plot of $\ln q_e$ versus $\ln C_e$.

The Temkin isotherm model³¹ is based on the adsorbent-adsorbate interactions and along with the saturation of adsorbent active sites, the adsorption energy decreases linearly rather than exponentially. The linear equation for Temkin isotherm model is as follows:

Table 3 Adsorption isotherm parameters for the removal of ARS onto PVC and PVC/CNT nanocomposite fibers.

Adsorbent	Langmuir isotherm model			Freundlich isotherm model			Temkin isotherm model		
	q_m (mg g^{-1})	b (L mg^{-1})	R^2	K_F ($\text{mg}^{1-1/n} \text{L}^{1/n} \text{g}^{-1}$)	n	R^2	A (L mg^{-1})	B	R^2
PVC	8.47	0.468	0.987	3.472	4.000	0.926	9.396	1.427	0.951
PVC/CNT	14.952	0.413	0.991	4.702	2.824	0.967	4.197	3.072	0.995

$$q_e = B \ln A + B \ln C_e \quad (6)$$

where A and B are the Temkin isotherm parameters, which are related to the equilibrium binding constant (L/mg) and the heat of adsorption (kJ/mol), respectively.

Table 3 lists the adsorption isotherm parameters calculated from their respective plots. The value of correlation coefficient (R^2) for Langmuir equation is higher for the PVC fibers while for PVC/CNT nanocomposite fibers, Temkin equation shows the highest R^2 value, suggesting that the Langmuir and Temkin isotherm models were found to be well representative of the adsorption equilibrium data.³²⁻³³

Furthermore, thermodynamic studies were performed to determine the adsorption mechanism of ARS onto PVC and PVC/CNT nanocomposite fibers. The values of thermodynamic parameters such as the standard free energy change (ΔG°), entropy change (ΔS°) and enthalpy change (ΔH°) associated with the adsorption processes were calculated using the following equations:

$$\Delta G^\circ = -RT \ln K_c \quad (7)$$

$$\ln K_c = \frac{\Delta S^\circ}{R} - \frac{\Delta H^\circ}{RT} \quad (8)$$

where, K_c and R are the distribution coefficient and gas constant ($8.314 \text{ J mol}^{-1} \text{ K}^{-1}$), respectively, and T is the temperature (K). The thermodynamic parameters were calculated from Fig. 9 and are listed in Table 4. The negative ΔH° suggested that the adsorption of ARS onto both type fibers was exothermic in nature. The negative

ΔS° values for both PVC and PVC/CNT nanocomposite fibers, showed a decrease in randomness at solid-solution interface. The positive ΔG° values suggest that the adsorption process was non-spontaneous and a low temperature favors the adsorption process. The energy associated with ΔG° for physical adsorption, physical adsorption along with chemical sorption and chemical sorption are in the ranges of -20 and 0 , -20 to -80 and -80 to 400 kJ/mol , respectively³⁴⁻³⁵. The values of ΔG° in Table 4 suggest that adsorption of ARS onto PVC and PVC/CNTs fibers was through physisorption.

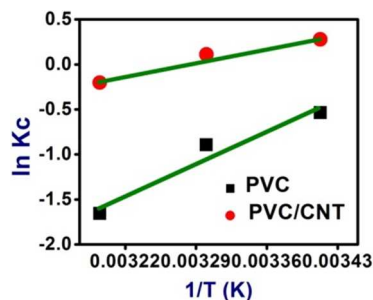


Fig. 9 Plot of $\ln K_c$ versus $1/T$ for PVC and PVC/CNT

nanocomposite fibers

Table 4 Thermodynamic parameters for the adsorption of ARS onto PVC and PVC/CNT nanocomposite fibers.

Adso rbent	ΔG° (kJ/mol)			ΔH° (kJ/mol)	ΔS° (J/mol K)	R^2
	30 °C	40 °C	50 °C			
PVC	1.306	2.255	4.311	-42.501	-148.9 0	0.963
PVC/ CNT	- 0.676	- 0.277	0.527	- 18.249	-59.75 2	0.950

Conclusions

PVC/CNT nanocomposite fibers were synthesized using a simple deposition technique. The adsorption, thermal, structural, and optical behaviors of the nanocomposite fibers was examined. The PVC/CNT nanocomposite fibers showed 81% enhancement in the surface area over the PVC fibers. The PVC/CNT nanocomposite fibers compared to the PVC fibers showed higher glass transition temperature. This also showed a lower optical band gap than PVC, which might be due to the formation of polarons within the

nanocomposite. Moreover, the PVC/CNT nanocomposite fibers compared to PVC showed two times higher adsorption capacity for the ARS. Owing to its enhanced adsorption capacity, surface area and better thermo-optical properties, this nanocomposite material is expected to find a suitable role in various practical applications.

Acknowledgements

This work was supported by the 2014 Yeungnam University Research Grant. This work was also supported by Priority Research Centers Program through the National Research Foundation of Korea (NRF) funded by the Ministry of Education (2014R1A6A1031189).

Notes and references

^aSchool of Chemical Engineering, Yeungnam University, Gyeongsan-si, Gyeongbuk 712-749, South Korea. Phone: +82-53-810-2512; Fax: +82-53-811-3262,

^bDepartment of Environmental Sciences, Faculty of Meteorology, Environment and Arid Land Agriculture, King Abdulaziz University, Jeddah, 21589, Saudi Arabia

^cCentral Metallurgical R & D Institute, Helwan, 11421, Cairo, Egypt

*Email: mynlee@ynu.ac.kr

†Electronic Supplementary Information (ESI) available: Sample preparation table, Band gap calculation table, Direct and indirect Optical band gap plots, XPS survey scans for PVC/CNT nanocomposite fibers.

- A. Guha, W. Lu, T. Zawodzinski and D. Schiraldi, *Carbon*, 2007, **45**, 1506–1517.
- H. Kong, C. Gao and D. Y. Yan, *Macromolecule*, 2004, **37**, 4022–4030.
- C. Park, Z. Ounaies, K. A. Watson, R. E. Crooks, J. J. Smith and S. E. Lowther *Chem. Phys. Lett.*, 2002, **364**, 303–308.
- Z. Jin, K. P. Pramoda, G. Xu and S. H. Goh, *Chem. Phys. Lett.*, 2001, **337**, 43–47.
- Z. Zhang, G. Chen, H. Wang and X. Li, *Chemistry an Asian Journal*, DOI: 10.1002/asia.201403100
- G. Sun, G. Chen, Z. Liu and M. Chen, *Carbon*, 2010, **48**, 1434.
- G. Sun, G. Chen, J. Liu, J. Yang, J. Xie, Z. Liu, R. Li and X. Li, *Polymer*, 2009, **50**, 5787.
- C. E. Wilkes, J. W. Summers, C. A. Daniels and M. T. Berard, *PVC handbook*, first ed., Hanser Verlag, Germany, 2005, 414–5.
- B. Ivan, T. Kelen and F. Tudos, *Degradation and stabilization of polymers*, Amsterdam, Netherlands, Elsevier Science, 1989, 483–714.
- T. Peprnicek, A. Kalendova, E. Pavlova, J. Simonik, J. Duchet, and J. F. Gerard, *Polym. Degrad. Stabil.*, 2006, **91**, 3322.
- J. Liu, G. Chen and J. Yang, *Polymer*, 2008, **49**, 3923.
- S. S. Sun, C. Z. Li, L. Zhang, H. L. Du and J. S. Burnell-Gray, *Polym. Int.*, 2006, **55**, 158.
- V. J. Mkhabela, A. K. Mishra and X. Y. Mbianda, *Carbon*, 2011, **49**, 610.
- V. Sajini, P. Jinu, M. Narahari and V. Suresh, *Carbon*, 2011, **49**, 198.
- T. Sterzynski, J. Tomaszewska, K. Piszczek and K. Skorczewska, *Compos Sci Technol*, 2010, **70**, 966-969.
- M. Hasan, A. N. Banerjee and M. Y. Lee, *J. Ind. Eng. Chem.* 2015, **21**, 828.
- X. L. Wu, P. Liu, T. Ramanathan, and A. A. Abdala, *eXPRESS Polym Lett.*, 2010, **4**, 723–728
- G. W. Becker, *Kolloid Z*, 1955, **140**, 1.
- M. Kawasumi, N. Hasegawa, M. Kato, A. Usuki and A. Okada, *Macromolecule*, 1997, **30**, 6333.
- M. Hasan and M. Y. Lee, *Progress in natural science Materials International*, 2014, **24**, 579.
- J. D. Lindberg and D.G. Synder, *Applied Optics*, 1973, **12**, 573.
- J. I. Pankove, *Optical Process in Semiconductors*, Printice-Hall, New Jersey, 1971
- E. Yousif, M. Abdullah, H. Hashim, N. Salih, J. Salimon and B. M. Abdullah, *Int. J. Ind. Chem*, 2013, **4**, 4.
- B. A. Hasan, M. A. Saeed and A. A. Hasan, *British J. Sci.*, 2012, **7**, 14.
- M. lamabla, in: second Mediterranean school on science and technology of advanced polymer-based materials, capri, 26 may, 1991.
- S. J. Gregg and K. S. W. Sing, *Adsorption, Surface Area and Porosity*, 2nd edn., Academic Press, London, 1982.
- Y. Wu, M. Zhang, H. Zhao, S. Yang and A. Arkin. *RSC Adv.*, 2014, **4**, 61256.
- V. K. Gupta, R. Kumar, A. Nayak, M.A. Barakat, and T. A. Saleh, *Advances in Colloid and Interface Science.*, 2013, **191**, 24-34.
- I. Langmuir, *J. Am. Chem. Soc.* 1918, **40**, 1361–1403.
- H. Freundlich, *J. Phys. Chem.*, 1907, **57**, 385–470.
- M. I. Temkin and V. Pyzhev, *Acta Physiochem. SSR*, 1940, **12**, 217–222]
- M. Ghaedi, A. Najibi, H. Hossainian, A. Shokrollahi and M. Soylak, *Toxicological & Environmental Chemistry*, 2012, **94**, 40-48.
- M. J. Iqbal and M. N. Ashiq, *J. Hazard Mater*, 2007, **139**, 57–66.
- M. J. Jaycock and G. D. Parfitt, *Chemistry of Interfaces*, Ellis Horwood Ltd, Onichester, 1981.
- R. Kumar, M. O. Ansari, and M. A. Barakat, *Ind. Eng. Chem. Res.*, 2014, **53**, 7167.